Effects of Magnetic Field and Heat Generation on Heat Transfer in Peristaltic Flow of Non-Newtonian Fluid in a Porous Channel

M M Hasan[1, 2, *], M A Samad[1], M M Hossain[1]

[1] Department of Applied Mathematics, University of Dhaka, Dhaka-1000, Bangladesh

[2] Department of Mathematics, Comilla University, Cumilla-3506, Bangladesh

Corresponding author's email: marufek@gmail.com

doi: https://doi.org/10.21467/proceedings.100.8

ABSTRACT

In the present study, we have discussed the heat transfer in peristaltic flow of non-Newtonian fluid in a porous asymmetric channel under the influence of magnetic field. The heat source term has been considered in this model which simulates heat generation. The governing equations of momentum and energy are simplified using long wave length and low Reynolds number approximation. The reduced equations have been solved numerically. Analytic solutions for stream function, velocity, temperature, pressure gradient and heat transfer coefficient are also obtained. The effects of various parameters are illustrated graphically and discussed from the physical point of view. The numerical results of heat transfer coefficient are also presented in tabular form and found to be in good agreement with previously published results. The trapping incident is also discussed here. It is noted that the size of the trapped bolus reduces for large value of Magnetic field parameter while opposite behavior is seen for permeability parameter.

Keywords: Heat generation, Trapped bolus, Temperature profile, Pressure gradient.

1 Introduction

In recent years, increasing attention has been bound for peristaltic flow with heat transfer. Peristaltic is an important mechanism for fluid transport in physiology and industry. This characteristic is naturally associated and occurred when a progressive wave of area contraction or expansion moving along the length of the filled channel. Peristaltic mechanism in channel has a wide range of physiological applications, for examples, urine transport from kidney to bladder, swallowing food material in esophagus, semen movement in the vas deferens of male reproductive tract and blood circulation in small blood vessels (Yildirim, Sezer 2010; Hamid *et al.* 2017; El-dabe *et al.* 2017). The initial work on peristaltic mechanism in a viscous fluid was conducted by Latham (1966) and after that we found many studies (Ahmed *et al.* 2018; Abd-Alla *et al.* 2013; Hayat *et al.* 2010; Misra, Sinha 2013; Elangovan, Selvaraj 2017).

It is known that blood carries a large quantity of heat to different parts of our body. When we work hard or when our body is exposed to severe heat situation then the blood flow of our body increases. Experiment shows that when the neighboring temperature crosses 20℃, heat transfer takes place from our skin surface and when the temperature is below 20℃, our body loses heat (Sinha *et al.* 2015). So, we can say that the study of heat transfer analysis is a significant area in connection with peristaltic flow. Such flows with heat transfer have many applications in biomedical sciences and industry such as analysis of tissues, blood oxygenation, dialysis, crude oil refinement, food processing and noxious fluid transport in nuclear industry (Ebaid 2008; Pandey, Tripathi 2011).

Proceedings DOI: 10.21467/proceedings.100; Series: AIJR Proceedings; ISSN: 2582-3922; ISBN: 978-81-942709-6-6 (eBook)

It is mentioned that most of the physiological and industrial fluids are non-Newtonian. On the other hand, the viscosity of non-Newtonian fluid varies with the rate of deformation. That means there is a non-linear relationship between them. For this reason, we cannot explain all non-Newtonian fluids in one constitutive equation. Thus, a number of non-Newtonian fluid models have been proposed (Nadeem *et al.* 2012). Casson fluid is one of the non-Newtonian fluids with a different character and was introduced by Casson (1959). Human blood can be presented by Casson's model (Blair *et al*. 1974). But little work is done regarding peristaltic flow of Casson fluid with heat transfer. The main goal is to study the heat transfer in peristaltic flow of non-Newtonian Casson fluid in a porous asymmetric channel with magnetic field and heat generation effects. The governing equations are reduced under low Reynolds number and long wave length approximations. The transformed equations have been solved analytically and numerically. The effects of various important parameters on velocity, pressure gradient and temperature are displayed graphically and discussed. Stream line patterns are also sketched.

2 Mathematical Formulation

Let us consider the peristaltic flow of non-Newtonian fluid in a porous and two-dimensional asymmetric channel of width $d_1 + d_2$. Here we choose a stationary frame of reference (X, Y) such that X measured along the axis of the channel and Y perpendicular to it. Let (U, V) be the velocity components in the stationary frame. The wall surfaces H_1 and H_2 of this asymmetric channel are maintained at constant temperatures T_0 and T_1 respectively. The porous channel is assumed to be homogenous. The motion is considered to be induced by a progressive sinusoidal wave train propagating with a constant speed c along the channel walls. An external uniform magnetic field of constant magnetic flux density $\bar{B} = (0, B_0)$ is applied along Y-axis. The geometry (in Fig.1) of the upper and lower wall surfaces are assumed to be

$$\left.\begin{aligned} Y = H_1 &= d_1 + a_1 cos\left\{\frac{2\pi}{\lambda}(X - ct)\right\} \\ Y = H_2 &= -d_2 - a_2 cos\left\{\frac{2\pi}{\lambda}(X - ct) + \phi\right\} \end{aligned}\right\} \qquad (1)$$

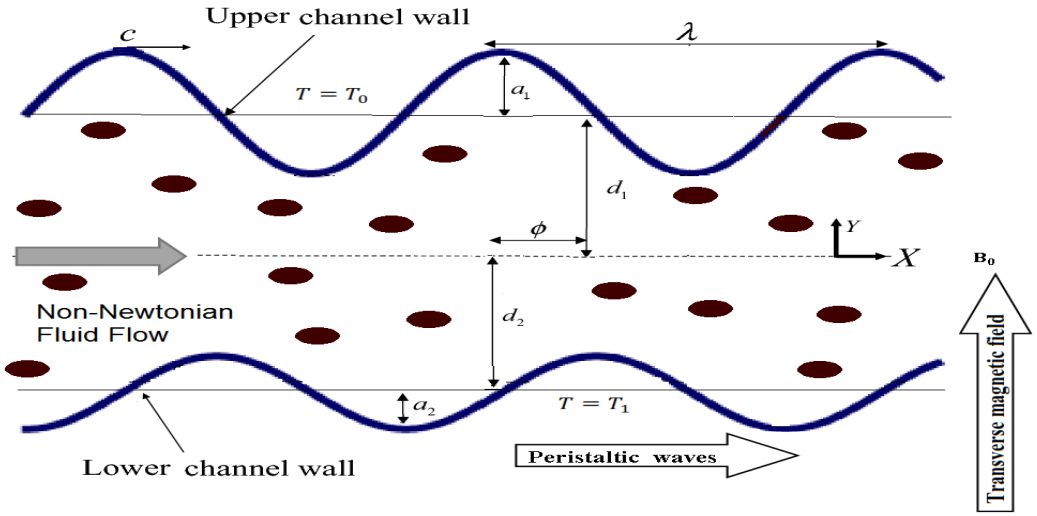

Fig.1 Geometry of model

where a_1, a_2 denote the waves amplitudes, λ is the wave length, t is the time, c is the velocity of propagation and ϕ is the phase difference $(0 \le \phi \le \pi)$, in which $\phi = 0$ corresponds to symmetric channel with waves out of phase and $\phi = \pi$ corresponds to waves in phase.

Then the constitutive equation for Casson fluid (Nakamura, Sawada 1988; El-dabe *et al*. 2001) is defined as

$$\tau_{ij} = 2\left(\mu_b + \frac{P_y}{\sqrt{2\pi}}\right)e_{ij} = 2\mu_b\left(1 + \frac{P_y}{\mu_b\sqrt{2\pi}}\right)e_{ij} = 2\mu_b\left(1 + \frac{1}{\beta}\right)e_{ij} \quad (2)$$

where $e_{ij} = \frac{1}{2}\left(\frac{\partial v_i}{\partial x_j} + \frac{\partial v_j}{\partial y_i}\right)$ is the $(i,j)^{\text{th}}$ component of deformation rate, τ_{ij} is the $(i,j)^{\text{th}}$ component of the stress tensor, π is the product of the component of deformation rate with itself, μ_b is the plastic dynamic viscosity, P_y is the yield stress, $\beta = \frac{\mu_b\sqrt{2\pi}}{P_y}$ is the Casson fluid parameter. For non-Newtonian Casson fluid flow $\mu = \mu_b + \frac{P_y}{\sqrt{2\pi}}$ which gives $\nu' = \nu\left(1 + \frac{1}{\beta}\right)$, where $\nu = \frac{\mu_b}{\rho}$ is the kinematic viscosity for Casson fluid. Again, for Newtonian case, the yield stress $P_y = 0$.

With all the above-mentioned considerations, the governing equations for of non-Newtonian Casson fluid are

$$\frac{\partial U}{\partial X} + \frac{\partial V}{\partial Y} = 0 \quad (3)$$

$$\frac{\partial U}{\partial t} + U\frac{\partial U}{\partial X} + V\frac{\partial U}{\partial Y} = -\frac{1}{\rho}\frac{\partial P}{\partial X} + \nu\left(1 + \frac{1}{\beta}\right)\left(\frac{\partial^2 U}{\partial X^2} + \frac{\partial^2 U}{\partial Y^2}\right) - \frac{\sigma B_0^2}{\rho}U - \nu\left(1 + \frac{1}{\beta}\right)\frac{U}{K'} \quad (4)$$

$$\frac{\partial V}{\partial t} + U\frac{\partial V}{\partial X} + V\frac{\partial V}{\partial Y} = -\frac{1}{\rho}\frac{\partial P}{\partial Y} + \nu\left(1 + \frac{1}{\beta}\right)\left(\frac{\partial^2 V}{\partial X^2} + \frac{\partial^2 V}{\partial Y^2}\right) - \nu\left(1 + \frac{1}{\beta}\right)\frac{V}{K'} \quad (5)$$

$$\frac{\partial T}{\partial t} + U\frac{\partial T}{\partial X} + V\frac{\partial T}{\partial Y} = \frac{k}{\rho C_p}\left(\frac{\partial^2 T}{\partial X^2} + \frac{\partial^2 T}{\partial Y^2}\right) + \frac{\nu}{C_p}\left(1 + \frac{1}{\beta}\right)\left[2\left\{\left(\frac{\partial U}{\partial X}\right)^2 + \left(\frac{\partial V}{\partial Y}\right)^2\right\} + \left(\frac{\partial U}{\partial Y} + \frac{\partial V}{\partial X}\right)^2\right] + \frac{Q'}{\rho C_p} \quad (6)$$

where B_0 is the uniform magnetic field strength, σ is the electric conductivity, ρ is the fluid density, C_p is the specific heat at constant pressure, k is the thermal conductivity, K' is the permeability of the porous channel, T is the temperature, Q' is the heat absorption/addition.

The corresponding boundary conditions are

$$\left.\begin{array}{llll} U = 0, & T = T_0, & \text{at} & Y = H_1 \\ U = 0, & T = T_1, & \text{at} & Y = H_2 \end{array}\right\} \quad (7)$$

In the stationary frame (X, Y) the flow is unsteady. But if observed in a co-ordinate system moving at the wave speed c in the wave frame (x, y), it can be considered as steady. The co-ordinates, velocity and pressure in two frames are related to

$$x = X - ct, y = Y, u = U - c, v = V, p(x,y) = P(X,Y,t), \bar{T}(\mathrm{x},\mathrm{y}) = T(X,Y,t) \quad (8)$$

where $u, v, p, \bar{T}$ are the velocity components, pressure and temperature respectively in the wave frame.

To minimize the complexity of the governing equations, the following non-dimensional variables are used.

$$\left.\begin{aligned} x' = \frac{x}{\lambda}\,, y' = \frac{y}{d_1}\,,\ u' = \frac{u}{c}\,,\ v' = \frac{v}{c\delta}\,,\ t' = \frac{ct}{\lambda}\,,\ p' = \frac{pd_1^2}{\lambda c\mu_b} \\ \delta = \frac{d_1}{\lambda}\,, h_1 = \frac{H_1}{d_1}, h_2 = \frac{H_2}{d_1}, d = \frac{d_2}{d_1}, a = \frac{a_1}{d_1}, b = \frac{a_2}{d_1}, \theta = \frac{\bar{T}-\bar{T}_0}{\bar{T}_1-\bar{T}_0} \end{aligned}\right\} \quad (9)$$

The governing equations $(3)-(6)$ under the assumptions of long wave length and low Reynolds number in terms of stream function ψ (dropping the das symbols) become

$$\frac{\partial p}{\partial x} = \left(1+\frac{1}{\beta}\right)\left[\frac{\partial^3\psi}{\partial y^3} - \alpha^2\left(\frac{\partial\psi}{\partial y}+1\right)\right] \quad (10)$$

$$\frac{\partial^4\psi}{\partial y^4} - \alpha^2\frac{\partial^2\psi}{\partial y^2} = 0 \quad (11)$$

$$\frac{\partial p}{\partial y} = 0 \quad (12)$$

$$\frac{\partial^2\theta}{\partial y^2} + \left(1+\frac{1}{\beta}\right)Br\left(\frac{\partial^2\psi}{\partial y^2}\right)^2 + Q_0 = 0 \quad (13)$$

The reduced boundary conditions are

$$\left.\begin{aligned} \psi = \frac{q}{2}, \quad \frac{\partial\psi}{\partial y} = -1, \quad \theta = 0, \quad \text{at } y = h_1 = 1 + acos2\pi x \\ \psi = \frac{-q}{2}, \quad \frac{\partial\psi}{\partial y} = -1, \quad \theta = 1, \quad \text{at } y = h_2 = -d - bcos(2\pi x + \phi) \end{aligned}\right\} \quad (14)$$

where $M = \sqrt{\frac{\sigma}{\mu_b}}B_0 d_1$ is the magnetic field parameter, $K = \frac{K'}{d_1^2}$ is the permeability parameter, q is the volume flow rate in the wave frame, $Pr = \frac{\rho\nu C_p}{k}$ is the Prandtl number, $Ec = \frac{c^2}{C_p(\bar{T}_1-\bar{T}_0)}$ is the Eckert number, $Br = Ec.Pr$ is the Brinkman number and $Q_0 = \frac{Q'd_1^2}{k(\bar{T}_1-\bar{T}_0)}$ is the heat generation parameter.

The dimensionless mean flow rate Q in the stationary frame is related to the dimensionless mean flow rate q in the wave frame by

$$Q = q + 1 + d \quad (15)$$

in which

$$q = \int_{h_2}^{h_1} u dy \quad (16)$$

Again, the heat transfer coefficient Z_1 at the upper wall is

$$Z_1 = h_{1x}\theta' = \frac{\partial h_1}{\partial x}\frac{\partial\theta}{\partial y} \quad (17)$$

3 Analytic solution

Exact solutions of the reduced equations along with the boundary conditions (14) were obtained by direct integration. The solutions of stream function ψ, velocity u, pressure gradient $\frac{dp}{dx}$ and temperature θ are

$$\psi = A_1 + A_2 y + A_3 e^{\alpha y} + A_4 e^{-\alpha y}$$

$$u = A_2 + A_3\alpha e^{\alpha y} - A_4\alpha e^{-\alpha y}$$

$$\frac{dp}{dx} = -(1 + 1/\beta)\alpha^2(A_2 + 1)$$

$$\theta = -D_1\alpha^4[D_2y^2 + D_3cosh(2\alpha y) + D_4sinh(2\alpha y)] - Q_0\frac{y^2}{2} + D_5y + D_6$$

where

$$\alpha = \sqrt{\frac{M^2}{1+1/\beta} + \frac{1}{K}}$$

$$A_1 = \frac{-(h_1 + h_2)[q\alpha cosh\frac{\alpha}{2}(h_1 - h_2) + 2sinh\frac{\alpha}{2}(h_1 - h_2)]}{2(h_1 - h_2)\alpha cosh\frac{\alpha}{2}(h_1 - h_2) - 4sinh\frac{\alpha}{2}(h_1 - h_2)}$$

$$A_2 = \frac{q\alpha cosh\frac{\alpha}{2}(h_1 - h_2) + 2sinh\frac{\alpha}{2}(h_1 - h_2)}{(h_1 - h_2)\alpha cosh\frac{\alpha}{2}(h_1 - h_2) - 2sinh\frac{\alpha}{2}(h_1 - h_2)}$$

$$A_3 = \frac{(h_1 - h_2 + q)sinh\frac{\alpha}{2}(h_1 + h_2)}{(h_1 - h_2)\alpha cosh\frac{\alpha}{2}(h_1 - h_2) - 2sinh\frac{\alpha}{2}(h_1 - h_2)}$$

$$A_4 = \frac{-(h_1 - h_2 + q)cosh\frac{\alpha}{2}(h_1 + h_2)}{(h_1 - h_2)\alpha cosh\frac{\alpha}{2}(h_1 - h_2) - 2sinh\frac{\alpha}{2}(h_1 - h_2)}$$

$$D_1 = Br(1 + 1/\beta), \quad D_2 = \frac{A_3^2 - A_4^2}{4}, \quad D_3 = \frac{A_3^2 + A_4^2}{8\alpha^2}, \quad D_4 = \frac{A_3A_4}{4\alpha^2}$$

$$D_5 = \frac{1}{h_2 - h_1} + \frac{D_1\alpha^4}{h_2 - h_1}\left[D_2\left({h_2}^2 - {h_1}^2\right) + D_3D_7 + D_4D_8\right] + \frac{Q_0}{2}(h_1 + h_2)$$

$$D_6 = -D_5h_1 + D_1\alpha^4\left[D_2{h_1}^2 + D_3cosh(2\alpha h_1) + D_4sinh(2\alpha h_1)\right] + \frac{Q_0}{2}h_1^2$$

$$D_7 = cosh(2\alpha h_2) - cosh(2\alpha h_1), \qquad D_8 = sinh(2\alpha h_2) - sinh(2\alpha h_1)$$

4 Numerical Solution

The transformed equations have also been solved numerically for different values of model parameters using MATLAB software (bvp4c function). Also the following data has been used: $a = 0.5$, $b = 0.6$, $d = 2$, $q = -2$, $x = 0$, $M = 1$, $K = 0.5$, $\beta = 1$, $\phi = \pi/4$ and $Q_0 = 0.2$, unless otherwise specified. The value of Prandtl number for human blood is $Pr = 21$ (Misra, Sinha 2013). So Pr is kept 21 in this study. Numerical computations have been carried out for various values of magnetic field parameter (M), Casson fluid parameter (β), permeability parameter (K), flow rate (q), heat generation parameter (Q_0) and Brinkman number (Br). The software ORIGIN has been used to show the numerical results graphically.

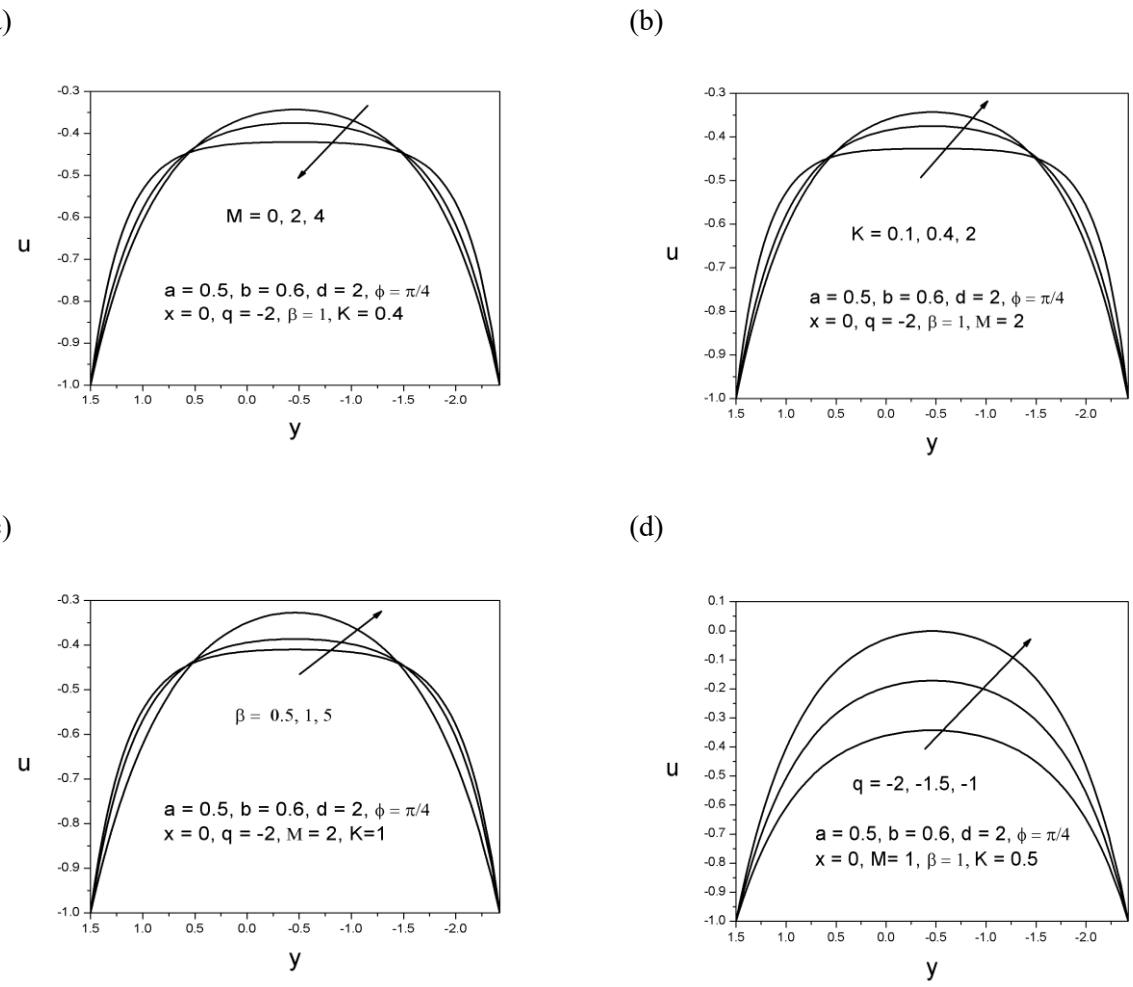

Fig.2 Velocity profiles for (a) magnetic field parameter, (b) permeability parameter, (c) Casson fluid parameter, (d) flow rate.

The behavior of magnetic field parameter M on velocity component u at the cross section $x = 0$ (at the inlet of the channel) is plotted in Fig. 2(a). It is mention that when M is increased, u decreases near the centre of the channel and increases in the neighborhood of the walls. The reason is that the applied magnetic field produces a resistive force to the flow and this force diminishes the velocity of the fluid. Fig. 2(b) is sketched to see the variation of velocity profiles for different values of permeability parameter K. It is evident from this figure that velocity is an increasing function of K. This is due to the fact that large K provides less resistance to the flow and accordingly there is a rise in the velocity of fluid near the middle of the channel. Again, an increase in velocity is noticed with increase in Casson fluid parameter β near the centre of the channel while opposite behavior is observed towards the walls as seen in Fig. 2(c). By definition, β is the ratio of plastic dynamic viscosity to yield stress. So, an increase in β means a decrease in yield stresses. This effectively accelerates the fluid flow. Fig. 2(d) shows that the velocity profile increased with an increase in flow rate q. This result is noticed that the greater amount of q will provide less resistance to the fluid flow and consequently there is an increase in the velocity of the fluid.

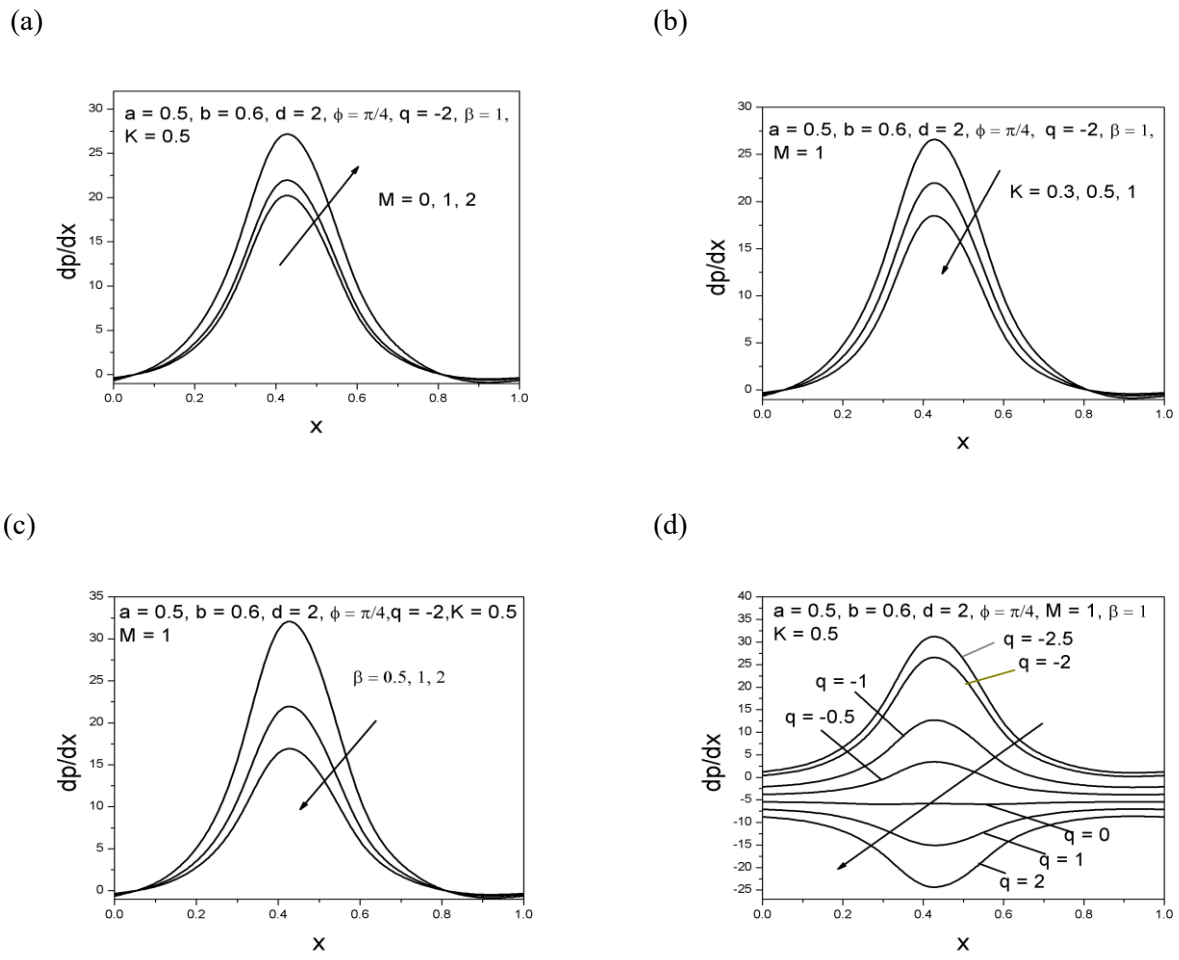

Fig.3 Pressure gradient profiles for (a) magnetic field parameter, (b) permeability parameter, (c) Casson fluid parameter, (d) flow rate.

The effects of M, K, β and q on pressure gradient dp/dx over one wave length $x \in [0,1]$ are displayed in Fig. 3. In Fig. 3(a), the pressure gradient dp/dx versus x is revealed for various values of M. This figure shows that as the values of M increases the magnitude of dp/dx is increases. That means when strong magnetic field is applied to the

flow field then higher-pressure gradient is needed to pass the flow in the channel. The effect of permeability parameter K on pressure gradient is presented in Fig. 3(b). It is observed that dp/dx reduces with increasing K. It is clear that when the value of K increases, the porosity of the channel reduces that indicates pressure is requires more when the porosity of the channel is enhanced. The pressure gradient for different values of Casson fluid parameter β is shown in the Fig. 3(c). It is noted that increasing β decreases the amplitude of pressure gradient. In practice, increasing β results in a decrease in yield stress of the fluid. Consequently, the fluid becomes less viscous and passes easily in the channel. The variation of dp/dx for different values of flow rate q is sketched in Fig. 3(d). It is clear that dp/dx decreases by increasing flow rate q.

Fig. 4 shows the temperature profile θ for different values of M, K, β, Br, Q_0 and q. Here we see that temperature profiles are almost parabolic in character and higher temperature is seen near the centre of the channel.

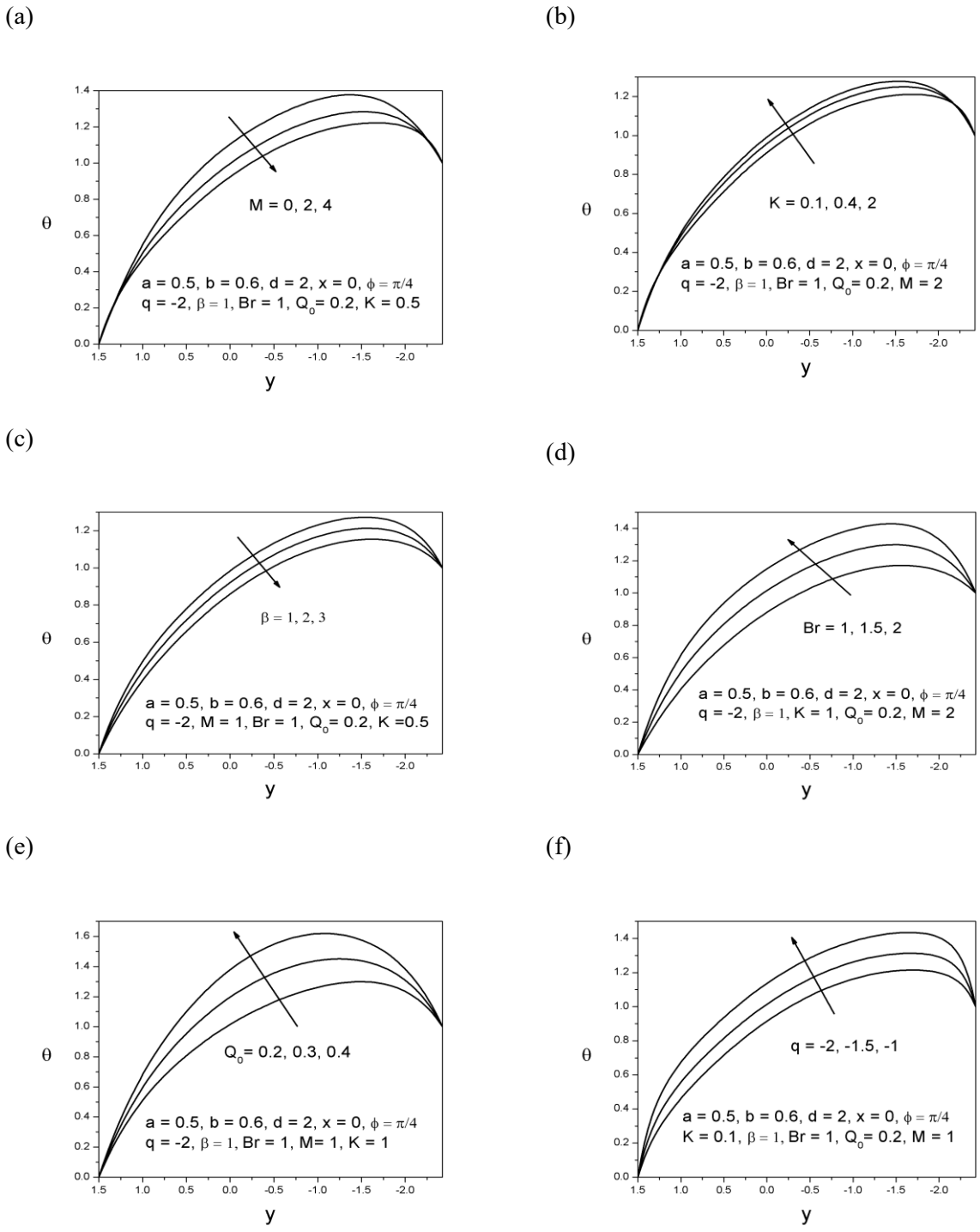

Fig.4 Temperature profiles for (a) magnetic field parameter, (b) permeability parameter, (c) Casson fluid parameter, (d) Brinkman number, (e) heat generation parameter, (f) flow rate.

Fig. 4(a) depicts that as M increased, the temperature profile falls due to resistance in fluid particle. Fig. 4(b) indicates that temperature increases as K increased. The influence of Casson fluid parameter β on temperature profiles is illustrated in Fig. 4(c). It reveals that temperature profile decreases with an increase in β. The effect of Brinkman number Br on temperature profiles is displayed in the Fig. 4(d). Here the temperature θ increases gradually with an increase in Br. Brinkman number $Br(= Ec.\Pr)$ represents the viscous effects which are due to energy production and thus heats up the fluid. Fig. 4(e) is plotted to represent the variation of temperature profiles for different values of heat generation parameter Q_0. It is clear from this figure that temperature profile increases for large values of Q_0. That means when heat generates during the fluid flow there is a significant increase in the thickness of thermal boundary layer. Again, an increase in flow rate q increases the temperature profiles as seen in the Fig. 4(f).

(a) $M = 1,\ \phi = 0$ (b) $M = 1,\ \phi = \pi/3$

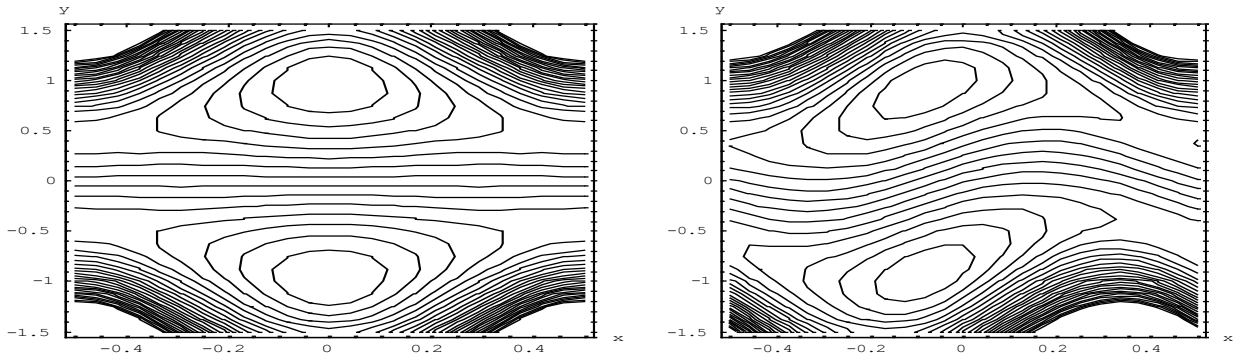

(c) $M = 3,\ \phi = 0$ (d) $M = 3,\ \phi = \pi/3$

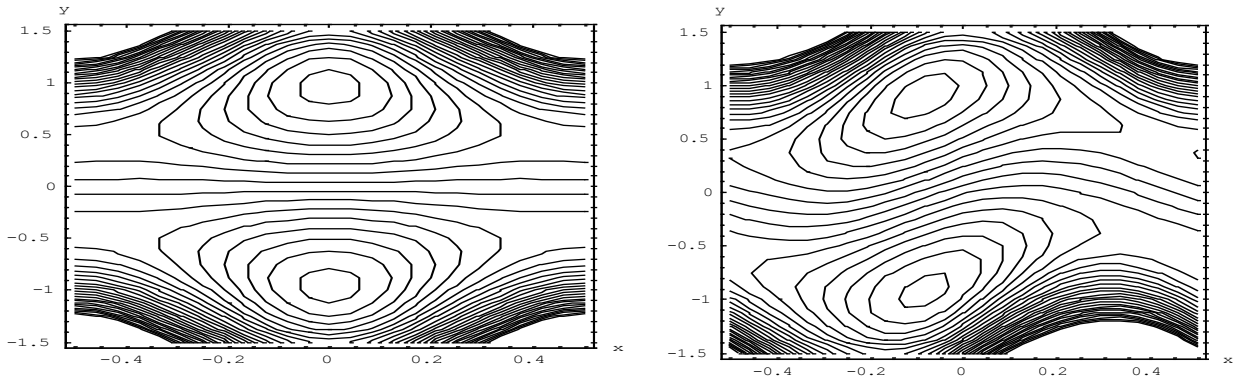

Fig.5 Streamlines for M in symmetric and asymmetric channels with

$$a = 0.5,\ b = 0.5,\ d = 1, q = -0.5,\ K = 1,\ \beta = 1.$$

Another attractive phenomenon is trapping for peristaltic flow. It is the formulation of contours of streamlines. To observe the effects of M, K, β and ϕ on streamlines in the symmetric and asymmetric channels we have sketched the Figs. 5-8. In the Figs. 5-7, the left panels (a) and (c) are related to symmetric channel and the right panels (b) and (d) are corresponded to asymmetric channel. It is noted from Fig. 5 that the size of the trapped bolus decreases with increase in M. Large M enhances the strength of magnetic field which increases the body force in the form of Lorentz force. This force causes the

resistance in the flow of the fluid. The influences of permeability parameter K on streamlines are discussed in the Fig. 6.

(a) $K = 0.8,\ \phi = 0$ (b) $K = 0.8,\ \phi = \pi/3$

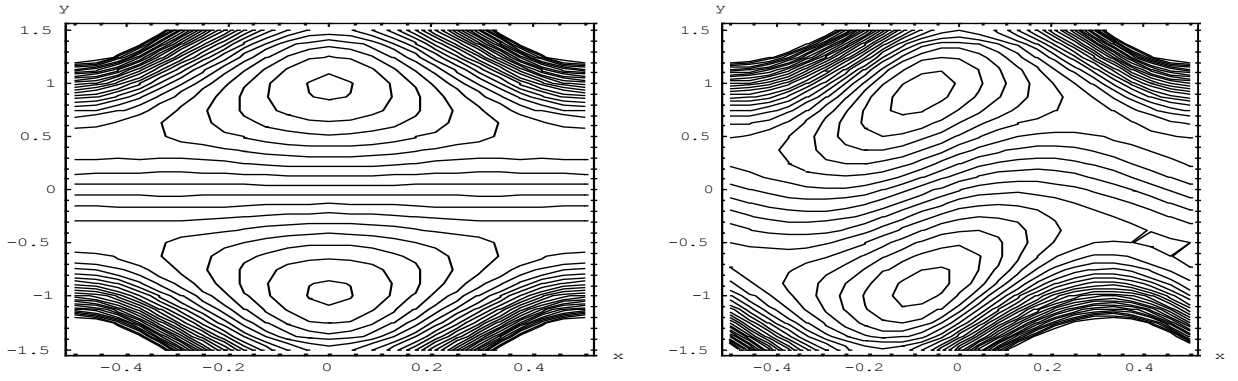

(c) $K = 2,\ \phi = 0$ (d) $K = 2,\ \phi = \pi/3$

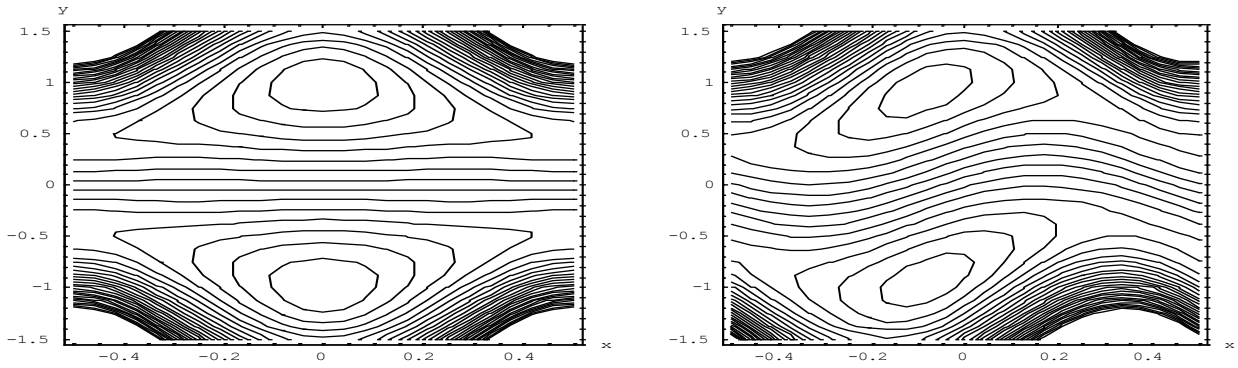

Fig.6 Streamlines for K in symmetric and asymmetric channels with

$$a = 0.5,\ b = 0.5,\ d = 1, q = -0.5,\ M = 1,\ \beta = 1.$$

The size of the trapped bolus magnifies with an increase in K. This result physically confirms the idea that peristaltic flow in a porous medium brings firmness of the fluid. Fig. 7 is sketched to see the variation of streamlines for different values of Casson fluid parameter β. It can be concluded that the volume of the trapping bolus increases with increasing β. Fig.8 shows the trapping characteristic for different values of phase difference ϕ for symmetric ($a = b, d = 1, \phi = 0$) and asymmetric channels. It is noted that the size of the trapped bolus decreases when ϕ increases and the trapping disappears when ϕ reaches to π. In addition, the bolus moves upward and decreases in size as ϕ increases.

(a) $\beta = 0.5,\ \phi = 0$ (b) $\beta = 0.5,\ \phi = \pi/3$

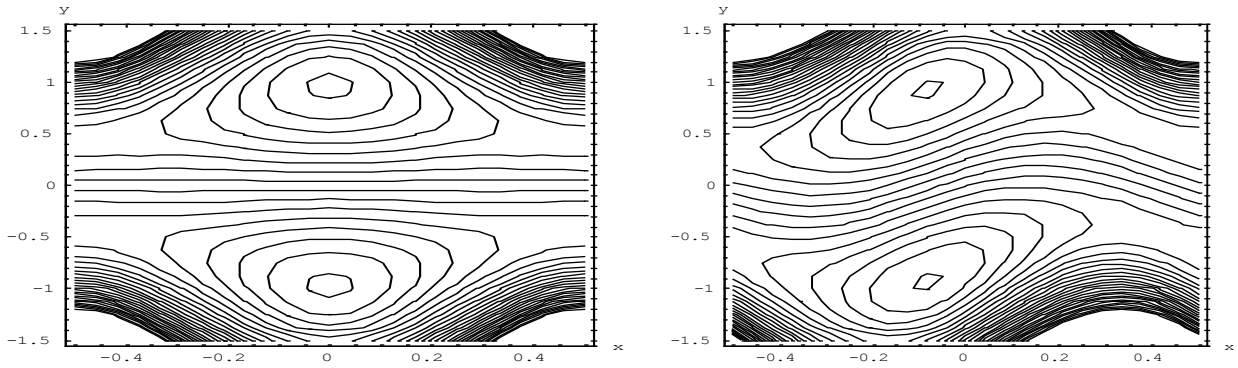

(c) $\beta = 2,\ \phi = 0$ (d) $\beta = 2,\ \phi = \pi/3$

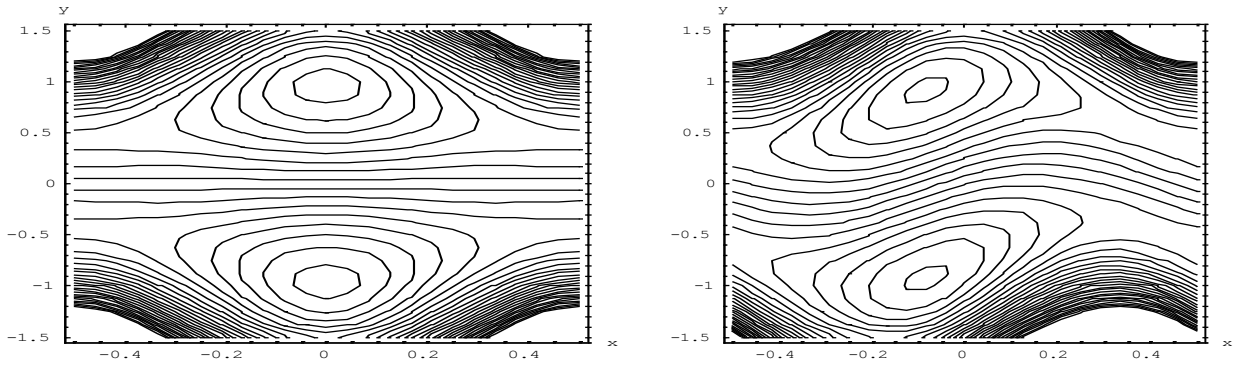

Fig.7 Streamlines for β in symmetric and asymmetric channels with $a = 0.5,\ b = 0.5,\ d = 1, q = -0.5,\ M = 1,\ K = 1.$

(a) $\phi = 0$ (b) $\phi = \pi/4$

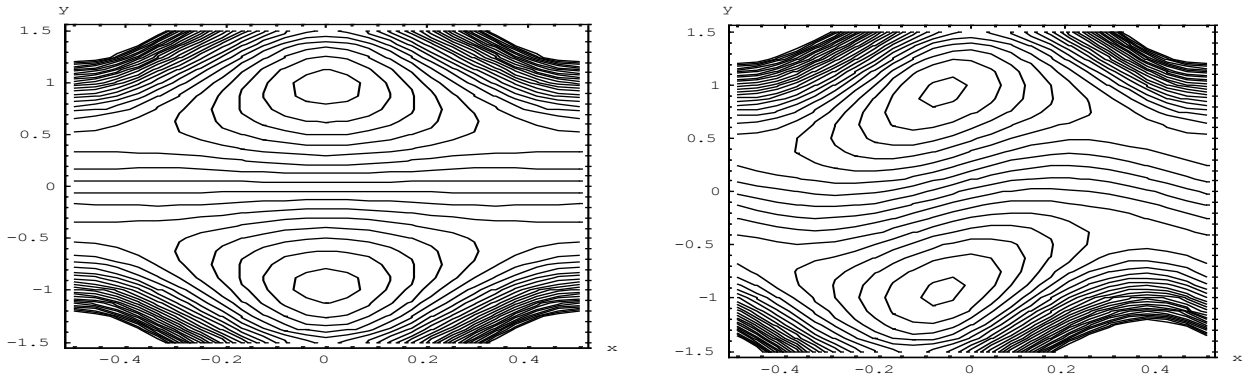

(c) $\phi = \pi/2$ (d) $\phi = \pi$

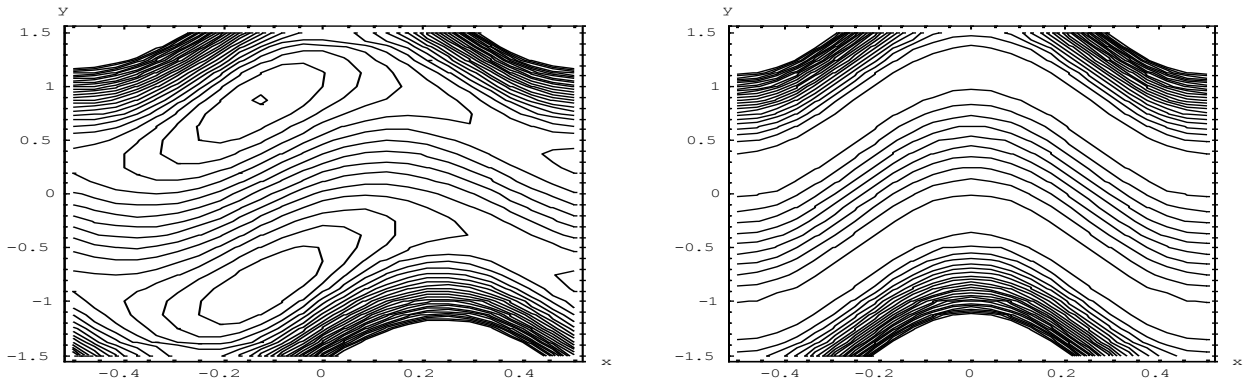

Fig.8 Streamlines for ϕ in symmetric and asymmetric channels with

$$a = 0.5,\ b = 0.5,\ d = 1, q = -0.5,\ M = 1,\ K = 1, \beta = 1.$$

Table1 gives a comparison between the numerical results obtained in the present study and the analytical results of previous study (Srinivas, Kothandapani 2008). To do so, both the studies have been brought to the same platform by considering equal parameters.

Table 1 Comparison of heat transfer coefficient Z_1 at upper wall for different values of Br (Newtonian Case)

$a = 0.5, b = 0.6, d = 1.5, M = 2, \phi = \pi/4, q = -2, 1/K = 0, 1/\beta = 0$				
x	Present	Srinivas,Kothandapani 2008	Present	Srinivas,Kothandapani 2008
	$Br(= Ec.Pr) = 1$		$Br(= Ec.Pr) = 2$	
0.1	1.0583	1.0586	1.5010	1.5013
0.2	1.4550	1.4556	1.6565	1.6569
0.3	1.7591	1.7596	1.8689	1.8692

5 Conclusion

The main findings of the study are

1. Velocity decreases at the central region of the channel and increases near the walls for increasing M. Also, reverse behaviors are seen for K and β.
2. An increase in Br results an increase in temperature profiles.
3. Heat generation parameter has increasing effect on temperature.
4. Higher pressure gradient is required to pass the flow for large M but opposite characteristics are observed for K, β and q.
5. The size of the trapped bolus reduces for large value of M while opposite property is noticed for K.

References

Abd-Alla, A.M., Abo-Dahab, S.M., Al-Simery, R.D.: Effect of rotation on peristaltic flow of a micropolar fluid through a porous medium with an external magnetic field. Journal of magnetism and Magnetic materials **348**, 33-43 (2013)

Ahmed, B., Javed, T., Ali, N.: Numerical study at moderate Reynolds number of peristaltic flow of micropolar fluid through a porous-saturated channel in magnetic field. AIP Advances **8**(1), 015319 (2018)

Blair, S., William, G., Spanner, D.C.: Introduction to biorheology by GW Scott Blair, Chapter XII on botanical aspects by DC Spanner, (1974)

Casson, N.: Rheology of disperse systems. Pergamon Press, London, **84**, (1959)

Ebaid, A.: Effects of magnetic field and wall slip conditions on the peristaltic transport of a Newtonian fluid in an asymmetric channel. Physics Letters A **372**(24), 4493-4499 (2008)

Elangovan, K., Selvaraj, K.: MHD peristaltic flow of blood through porous medium with slip effect in the presence of body acceleration. World Journal of Modelling and Simulation **13**(2), 151-160 (2017)

El-dabe, N.T.M., Abou-zeid, M.Y., Younis, Y.M.: Magnetohydrodynamic peristaltic flow of Jeffry nanofluid with heat transfer through a porous medium in a vertical tube. Applied Mathematics & Information Sciences, **11**(4), 1097-1103 (2017)

El-dabe, N.T.M., Saddeck, G., El-Sayed, A.F.: Heat transfer of MHD non-Newtonian Casson fluid flow between two rotating cylinders. Mechanics and Mechanical Engineering **5**(2), 237-251 (2001)

Hamid, A. H., Tariq Javed, Ahmed, B., Ali, N.: Numerical study of two-dimensional non-Newtonian peristaltic flow for long wavelength and moderate Reynolds number. Journal of the Brazilian Society of Mechanical Sciences and Engineering **39**(11), 4421-4430 (2017)

Hayat, T., Hina, S., Ali, N.: Simultaneous effects of slip and heat transfer on the peristaltic flow. Communications in Nonlinear Science and Numerical Simulation **15**(6), 1526-1537 (2010)

Latham, T.W.: Fluid motion in a peristaltic pump. MS thesis, MIT Cambridge, MA, (1966)

Misra, J.C., Sinha, A.: Effect of thermal radiation on MHD flow of blood and heat transfer in a permeable capillary in stretching motion. Heat Mass Transfer **49**(5), 617-628 (2013)

Nadeem, S., Rizwan Ul Haq, Lee, C.: MHD flow of a Casson fluid over an exponentially shrinking sheet. Scientia Iranica **19**(6), 1550-1553 (2012)

Nakamura, M., Sawada, T.: Numerical study on the flow of a non-Newtonian fluid through an axisymmetric stenosis. Journal of Biomechanical Engineering **110**(2), 137-143 (1988)

ISBN: 978-81-942709-6-6 ISSN: 2582-3922

Pandey, S.K., Tripathi, D.: A mathematical model for swallowing of concentrated fluids in oesophagus. Applied Bionics and Biomechanics **8**, 309-321 (2011)

Sinha, A., Shit, G.C., Ranjit, N.K.: Peristaltic transport of MHD flow and heat transfer in an asymmetric channel: Effects of variable viscosity, velocity-slip and temperature jump. Alexandria Engineering Journal, **54**(3), 691-704 (2015)

Srinivas, S., Kothandapani, M.: Peristaltic transport in an asymmetric channel with heat transfer-A note. International Communications in Heat and Mass Transfer **35**, 514-522 (2008)

Yildirim, A., Sezer, S.A.: Effects of partial slip on the peristaltic flow of a MHD Newtonian fluid in an asymmetric channel. Mathematical and Computer Modelling **52**, 618-625 (2010)